Experimental and theoretical analysis on ultraviolet 370 nm AlGaInN light-emitting diodes

2006 Semicond. Sci. Technol. 21 598

(http://iopscience.iop.org/0268-1242/21/5/005)

INSTITUTE OF PHYSICS PUBLISHING SEMICONDUCTOR SCIENCE AND TECHNOLOGY

Semicond. Sci. Technol. **21** (2006) 598–603 doi:10.1088/0268-1242/21/5/005

Experimental and theoretical analysis on ultraviolet 370 nm AlGaInN light-emitting diodes

Yi-An Chang[1], Sheng-Horng Yen[2], Te-Chung Wang[1], Hao-Chung Kuo[1], Yen-Kuang Kuo[2], Tien-Chang Lu[1] and Shing-Chung Wang[1]

[1] Institute of Electro-Optical Engineering, National Chiao-Tung University, Hsinchu, 300, Taiwan

[2] Department of Physics, National Changhua University of Education, Changhua, 500, Taiwan

E-mail: rayman0313.eo92g@nctu.edu.tw

Received 14 October 2005, in final form 10 February 2006
Published 21 March 2006
Online at stacks.iop.org/SST/21/598

Abstract

An ultraviolet (UV) AlGaInN light-emitting diode (LED) with 370 nm emission is demonstrated. At room temperature (RT) UV power of 0.8 mW at 20 mA with 3.6 V operation voltage is achieved. It provides 4 mW output when driven at 125 mA under continuous-wave (CW) operation. Qualitative optimization of the Al composition in the AlGaN electron-block layer and the quaternary AlGaInN quantum well (QW) number of the UV LED is also investigated in this study. The numerical results fit with the experimentally demonstrated output performance of our AlGaInN UV LED. We find that the UV AlGaInN LED can provide better output characteristics when the Al composition in the AlGaN electron-block layer is in the range 19–21% and the AlGaInN QW number is in the range 5–7 by reducing the electron leakage current.

1. Introduction

III–V nitride-based emitters had been unmitigatedly developed in the ultraviolet–violet–blue region of the spectrum for potential applications in illuminated devices, laser diode light sources for high-density optical storage system, full-colour display and medical applications. Highly efficient LEDs with ultraviolet–violet–blue and white emission were commercially available. Especially, UV LEDs have recently attracted much attention as a strong candidate in biological agent detection and transceivers for converting nonlinear-of-sight optical communications. AlGaN or quaternary AlGaInN are expected to be applied as the QW active region in UV LEDs due to the naturally direct high-bandgap transition. However, the illuminated power and efficiency of the UV LEDs are much worse than those of the visible LEDs, which had been observed due to some factors including defects in the QW active region, device heating under CW operation and especially carrier leakage from the active region. The amount of leakage current in UV LEDs increases vastly when increasing the Al composition in the QW to obtain deep UV emission. Significant progress with UV LEDs has been made in the emission wavelength region 325–400 nm with mW output [1–4]. For UV LEDs with an emission wavelength of 267 nm, AlGaN-based LEDs, with a pulse operation output power of 4.5 mW and 165 μW at 435 mA under CW operation for an array of four LEDs in parallel, have been demonstrated by Yasan *et al* [5]. For 365 nm UV LEDs, with the use of laser-induced liftoff and polishing technologies, Morita *et al* have obtained an output power of 100 mW with an external quantum efficiency of 5.6% at 500 mA [6]. On the other hand, with an emission wavelength shorter than the characteristic wavelength corresponding to the GaN bandgap, Nishida *et al* adopted a short period alloy superlattice as p-type cladding and p-type contact layers to have a transparent 348–351 nm LED with 7 mW output at 220 mA [7].

These efforts have resulted in UV LEDs having an acceptable output characteristic; however, it needs to be mentioned that substantial work is necessitated with an aim to improve the emitting power and efficiency. For a 370 nm

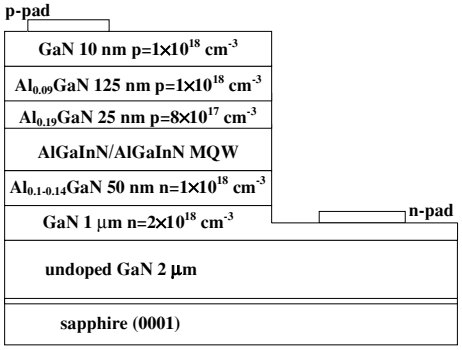

Figure 1. Schematic plot of the AlGaInN/AlGaInN LED structure under study.

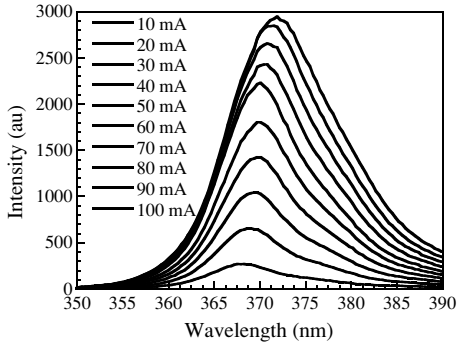

Figure 2. EL spectrum of the UV AlGaInN LED under CW operation when the input current is in the range 10–100 mA.

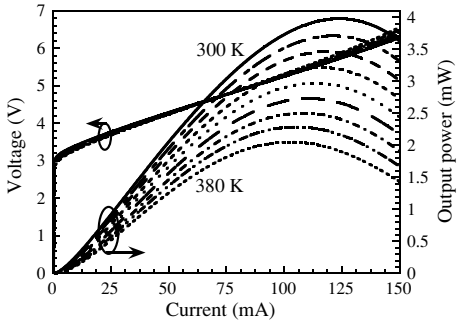

Figure 3. Output characteristic of the UV LED when the device temperature is varied in the range 300–380 K.

UV LED, the use of a quaternary AlGaInN QW active region is beneficial for obtaining better material quality and higher internal quantum efficiency [8]. Zhang *et al* had also pointed out that the use of quaternary AlGaInN as barriers could drastically improve the heterostructure quality [9]. In this work, we present the growth and fabrication of UV LEDs operating at 370 nm based on a quaternary AlGaInN QW active region. To create a more efficient UV LED, we further theoretically investigate the relationship of the Al composition in the AlGaN electron-block layer and the QW number to the LED output performance, with an aim to reduce the electron leakage current.

2. Device fabrication and characteristics

Figure 1 depicts the AlGaInN/AlGaInN LED structure under study. The LEDs used in this study were grown on a c-face sapphire substrate by low-pressure horizontal-flow metalorganic chemical vapour deposition (MOCVD) using a 30 nm thick low-temperature GaN nucleation layer at 550 °C, followed by a 2 μm thick high-temperature undoped GaN buffer layer and a 1 μm thick Si-doped GaN to form the n-contact layer at 1050 °C. Next, a 50 nm thick graded n-type $Al_xGa_{1-x}N$ ($x = 0.1$–0.14) was deposited for cladding. Then, the growth temperature was linearly decreased to 850 °C to grow the active region of the UV LED. The active region consisted of three quaternary $Al_{0.06}Ga_{0.85}In_{0.09}N$ multiple QWs sandwiched by four $Al_{0.05}Ga_{0.94}In_{0.01}N$ barriers. The temperature was afterwards increased to 1050 °C for growing a 25 nm thick p-type $Al_{0.19}Ga_{0.81}N$ electron-block layer, followed by a 125 nm thick p-type $Al_{0.09}Ga_{0.91}N$ and a 10 nm thick p-GaN contact layer to complete the structure.

After MOCVD growth, the fabrication process began by partially etching by reactive ion etching from the surface of the p-type GaN contact layer until the n-type GaN was exposed. Ni/Au metal was evaporated onto the p-type GaN and Ti/Al metal was evaporated onto the n-type GaN. The chip size was 300×300 μm^2 and was formed by packing into 5 mm lamps with a standard process for output characteristic measurement.

The device characteristics were obtained with a probe station, Keithlyn 238 current source and Newport 1835C power meter module. The electroluminescence (EL) spectrum was measured by an Advantec optical spectrum analyser (OSA) with a 0.1 nm spectrum resolution. Figure 2 shows the EL spectrum of the UV AlGaInN LED under CW operation when the input current is in the range 10–100 mA. The main peak of the emission wavelength designed slightly longer than 365 nm is for the purpose of preventing strong internal absorption by the bulk GaN, and it shifts from 368 nm to 372 nm with increased input current from 10 mA to 100 mA. Figure 3 shows the output characteristic of the UV LED when the device temperature is varied in the range 300–380 K. During the measurement of the temperature-dependent output characteristics, the UV LED is mounted on a hot plate and the device temperature is monitored with a thermal coupler. The RT UV power of the LED is near 0.8 mW at 20 mA with 3.6 V operation voltage and increased to 4 mW when the LED is driven at 125 mA under CW operation. The wall plug efficiency is approximately 1.1% and the external quantum efficiency is 1.2%. When the device temperature is operated at 380 K, the UV LED can still provide 0.5 mW output when the input current is 20 mA. A maximum output power of 2.1 mW can be achieved at 380 K when the input current is 100 mA.

For blue and green LEDs, which are made by III-nitride materials, the reports have shown that the main peak of the emission wavelength decreases first and increases afterward as the input current is increased. This phenomenon is found to be attributed to the localized states resulting from indium inhomogeneity. However, there is no short-wavelength shift in our UV AlGaInN LED. It is supposed that the indium composition in the AlGaInN QW is much less than that in the blue or green LEDs and the segregation of indium cannot dominate under this situation.

3. Theoretical analysis

It is universally known that qualitatively theoretical analysis can advantageously provide a way to realize the output characteristic of the optoelectronic semiconductor device. Numerical simulation is always required to model and optimize the output characteristic of the device. In this study, the numerical simulation is executed with the use of an advanced physical model of semiconductor devices (APSYS) [10], which is utilized as a full two-dimensional simulator that solves the Poisson's equation, current continuity equations, photon rate equation and scalar wave equation, and accounts for current spreading in this specific study. In the gain model, material gain and loss for both bulk and QW as functions of wavelength and carrier density are computed. Due to the lower value of dielectric constant in wide-bandgap III–V nitride materials, the optical gain of AlGaInN QW structure is calculated by the Coulomb-enhanced gain spectral function [11]:

$$g(\hbar w) = \text{real}\left\{\int_{E_{g_0}}^{\infty} \frac{g_0(E_{cv})}{1 - q_1(E_{cv}, \hbar w)}\left[1 - i\frac{E_{cv} - \hbar w}{\Gamma_{cv}}\right] \times L(\hbar w - E_{cv})\,\mathrm{d}E_{cv}\right\}, \tag{1}$$

in which

$$q(E_{cv}, \hbar w) = \frac{-ia_0 E_0 E_{cv}}{\pi k |M_{ji}(E_{cv})|}\int_0^{\infty} \mathrm{d}k'\, k' \frac{|M_{ji}(E_{cv'})|}{E_{cv'}} \times \frac{f_e(E_{cjk'}) + f_h(E_{vjk'}) - 1}{\Gamma_{cv} + i(E_{cv} - \hbar w)} \times \Theta(k, k'), \tag{2}$$

$$\Theta(k, k') = \int_0^{2\pi} \mathrm{d}\theta \frac{1 + C_{pl} k a_0 q^2 / 32\pi N_{2D}}{1 + q/k + C_{pl} k a_0 q k^3 / 32\pi N_{2D}}, \tag{3}$$

and

$$q^2 = k^2 + k'^2 - 2kk' \cos\theta, \tag{4}$$

where θ is the angle between in-plane vectors k and k', $g_0(E_{cv})$ is the spectral wavefunction, which consists of a sum of $g_{ji}(E_{cv})$ contributions from transitions between jth-subband electrons and ith-subband holes, Γ_{cv} represents the Lorentzian width and equals to $\hbar/\tau_{cv}$, which is simplified without considering the dependence upon $\hbar w$ and E_{cv} energies in the calculations, a_0 is the exciton Bohr radius given by $4\pi\hbar^2\varepsilon_b\varepsilon_0/e^2 m_{rj}$, E_0 is the corresponding Rydberg energy, E_{cv} is specified by $E_{cv}(k) = E_g + \Delta E_g + E_{cjk} + E_{vik}$ where E_{cjk} and E_{vik} are electron and hole energies from jth-subband of conduction band and ith-subband of valence band in the QW active region, $|M_{ji}|^2$ is the transition matrix element, C_{pl} is a unitless constant typically in a range 1–4, and $N_{2D} = n \times$ (QW thickness) is the two-dimensional carrier density in the QW. The gain spectrum is broadened by the Lorentzian function.

In the optical mode model, all modes are treated as possible since they all contribute to the emission power because of the non-coherent nature of spontaneous emission. The photon rate equation, which couples to the drift–diffusion equations, is also solved. Complex refractive indices computed from the material gain are required as input. For the numerical simulation, based on the $k \cdot p$ theory, a Hamiltonian matrix of the Luttinger–Kohn type and an envelope function approximation are used to solve the AlGaInN QW subband structures. A self-consistent carrier density model [10, 12], which is given by

$$n_{2D}(x, y) = \sum_j g_n^j(y)\rho_j^0 kT \ln\{1 + \exp[(E_{fn}(x, y) - E_j)/kT)]\}, \tag{5}$$

is used to solve the piezoelectric field in the QW, where the subscript j denotes all confined states, $g_n^j(y)$ is the electron wavefunction assuming that the well is parallel to x-axis, ρ_j^0 is the two-dimensional density of states and E_j is the confined level. For this specific simulation, the temperature-dependent bandgap energies of binary InN, GaN and AlN alloys are governed by the Varshni equation and the bowing factors of ternary GaInN, AlGaN and AlInN alloys are 2.4, 0.7 and 2.5 eV, respectively [13, 14]. Most Luttinger-like valence band parameters that we used in this study such as $A_1, A_2, \ldots, A_6$ for nitrides and the deformation potentials, elastic constants, etc are also obtained from [13], except that the electron and hole mobilities are taken from the default database values given in the APSYS material macro file [10].

For the treatment of device heating, the thermoelectric power and thermal current induced by temperature gradient are solved utilizing the methods provided by Wachutka *et al* [15–17]. Various heat sources, including Joule heat, generation/recombination heat, Thomson heat and Peltier heat, are taken into account in this specific study. The boundary temperature between the LED contacts and the ambiance is solved assuming that the contacts are connected to a thermal conductor with a fixed temperature set by the simulator. The calculation of the interface charge density including spontaneous and piezoelectric polarization in the ternary III-nitride material as a function of composition and microscopic structure is done by the use of *ab initio* density-functional techniques and the Berry phase method [18], while we assume that the charges at multiple QWs are with partial 85% screening. For the interface charge of the quaternary AlGaInN QW, it is predicted by the ternary interpolation formulae [19]

$$D_{\text{charge}}\text{Al}_x\text{Ga}_y\text{In}_z\text{N} = \frac{xy D_{\text{charge}}(\text{Al}_u\text{Ga}_{1-u}\text{N})}{xy + yz + zx} + \frac{yz D_{\text{charge}}(\text{Ga}_y\text{In}_{1-y}\text{N})}{xy + yz + zx} + \frac{zx D_{\text{charge}}(\text{In}_w\text{Al}_{1-w}\text{N})}{xy + yz + zx},$$
$$z = 1 - x - y, \quad u = \frac{1 + x - y}{2}, \quad v = \frac{1 + y - z}{2}, \quad w = \frac{1 + z - x}{2}. \tag{6}$$

The numerical spontaneous emission rate spectrum of the UV AlGaInN LED as a function of the input current is shown in figure 4. The inset in figure 4 depicts the main peaks of the numerical spontaneous emission rate spectra and the experimental EL spectra. It is clearly seen that the main peaks of the numerical spontaneous emission rate spectra and the experimental EL spectra are of good agreement. The spontaneous emission rate calculated in this study is given by [20]

$$r_{\text{sp}}^{\text{qw}}(E) = \sum_{i,j}\left(\frac{2\pi}{\hbar}\right)|H_{ij}|^2 f_j(1 - f_i)D(E)\rho_{ij}, \tag{7}$$

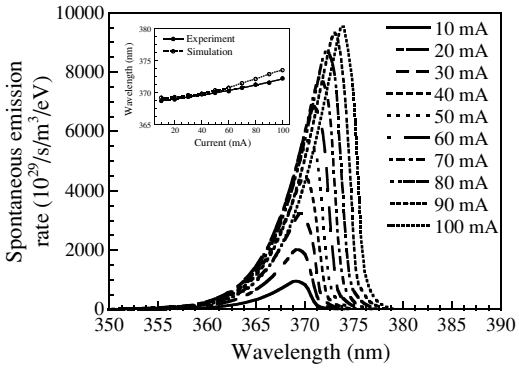

Figure 4. Numerical spontaneous emission rate spectrum of the UV AlGaInN LED as a function of the input current. The inset shows the main peaks of the numerical spontaneous emission rate spectra and the experimental EL spectra.

where

$$|H_{ij}|^2 = \left(\frac{q}{m_0}\right)^2 \left(\frac{2\hbar w}{4\varepsilon_1 \varepsilon_0 \omega^2}\right) M_{ij}^2, \tag{8}$$

and

$$\rho_{ij} = \rho_{ij}^0 \cdot h\big(\hbar\omega - E_{ij}^0\big), \tag{9}$$

and f_i, f_j represent the Fermi functions for the ith and jth levels. $D(E)$ is the optical mode density. The spontaneous emission power (P_{spon}) is calculated by the integral of all modes spontaneity:

$$P_{\text{spon}}(w)\Delta w = A \int_0^L \mathrm{d}z_s \big(\hbar w \cdot r_{\text{sp}}^{\text{qw}}(E)\big)\Delta E, \tag{10}$$

and the extracted output power from the LED top surface is

$$P_L(w)\Delta w = \sum_{ny} \big(1 - r_1^2\big)\frac{n_g}{n}\frac{L_x g_l}{k} \int_0^L |Z_2(z_s)|^2 \,\mathrm{d}z_s(\hbar w) \times \langle n|r_{\text{sp}}^{\text{qw}}(E)|n\rangle \cdot \Delta E, \tag{11}$$

where A is the active region cross section in the LED and we regard the LED as a special case of the Fabry–Perot laser with a cavity length of L. n and n_g are the indices, and g_l is a integral constant. We wish to underscore that the package loss assumed in this study is zero, and therefore the ratio of P_L/P_{spon} gives the LED external efficiency. A current efficiency can also be obtained from the ratio of the spontaneous recombination current (I_{spon}) to the total current, which is the sum of the spontaneous recombination current, nonradiative recombination current (I_{nr}) and leakage current (I_{leak}):

$$\eta_{\text{curr}} = \frac{I_{\text{spon}}}{I_{\text{spon}} + I_{\text{nr}} + I_{\text{leak}}}. \tag{12}$$

Figure 5 shows the numerical temperature-dependent output characteristics of the UV AlGaInN LED. To fit the experimental LED output characteristic, some parameters are used such as the radiative recombination coefficient for the bulk AlGaInN, AlGaN, GaN is 2.9 × 10^{-15} m^3 s^{-1}, the auger coefficients for n and p carrier are both set to 4 × 10^{-40} m^6 s^{-1}, and the carrier lifetime is 1 ns [21]. A large internal loss value of 1000 m^{-1} is assumed due to the large defect density in III–V nitride material. It is clearly seen that the temperature-dependent light output versus current (*L–I*)

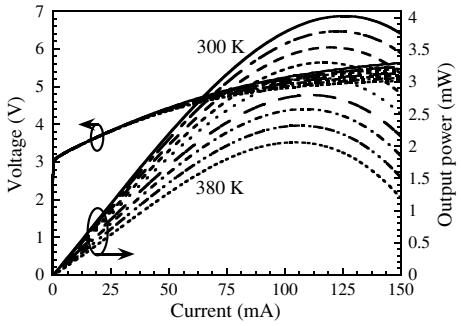

Figure 5. Numerical temperature-dependent output characteristics of the UV AlGaInN LED.

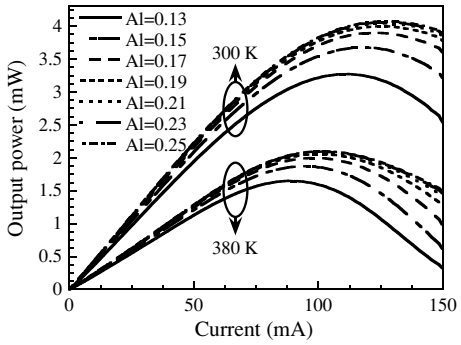

Figure 6. *L–I* characteristics of the UV AlGaInN LED with variant Al compositions in AlGaN electron-block layer when the device temperatures are 300 K and 380 K.

characteristic obtained numerically fits in with the experiment despite that the differential resistance is slightly inconsistent. Practically, the characteristics of the UV AlGaInN LED can be quantitatively analysed by the simulator with the parameters shown above, which remain unchanged throughout the study. To enhance the output power of the UV AlGaInN LED, we further investigate the effects of the aluminium composition in the AlGaN electron-block layer and the QW number on the UV AlGaInN LED, with an aim to reduce the electron leakage current and therefore improve the output power.

Several reports have shown that the electron leakage current plays an important role in the III–V nitride material due to the large discrepancy of electron and hole effective masses and the low p-type doping concentration [22–27]. For UV LEDs with an emission wavelength of 305–365 nm, the Al composition in the AlGaN electron-block layer is typically in the range 23–70% [28–31]. When the emission wavelength is shorter, the Al composition in the AlGaN electron-block layer shall be increased because the conduction band offset is decreased and more electrons overflow to the p-type layers. Figure 6 shows the *L–I* characteristics of the UV AlGaInN LED with variant Al compositions in the AlGaN electron-block layer when the device temperatures are 300 K and 380 K. It is observed that the output power is enhanced when the Al composition in the AlGaN electron-block layer is increased, and the output power at 300 K is limited when the Al composition in the AlGaN electron-block layer is higher than 19%. For the UV LED operated at 380 K, increasing the Al composition in the AlGaN electron-block layer to be higher than 19% can also

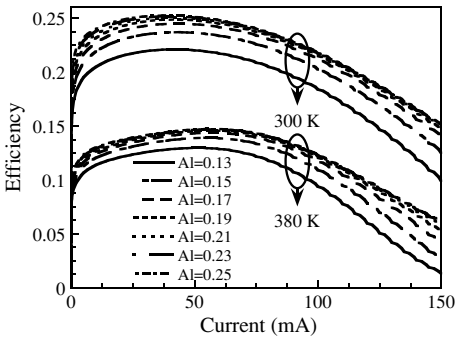

Figure 7. Current efficiency of the UV AlGaInN LED as a function of the input current for variant Al compositions in the AlGaN electron-block layer when the device temperatures are 300 K and 380 K.

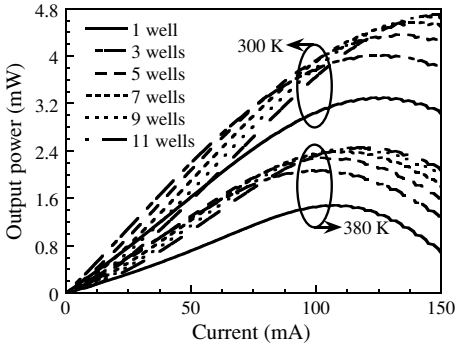

Figure 8. *L–I* characteristic of the UV AlGaInN LED with variant QW numbers when the device temperatures are 300 K and 380 K.

effectively prevent electron overflow and the output power remains unchanged when the input current is lower than 110 mA.

Figure 7 shows the current efficiency of the UV AlGaInN LED as a function of the input current for variant Al compositions in the AlGaN electron-block layer when the device temperatures are 300 K and 380 K. Increasing device temperature with decreased internal efficiency is found due to the increase of recombination loss and carrier leakage from the active region. With higher input current and higher device temperature, the electron leakage current and the nonradiative recombination increase which in turn results in reduction in current efficiency. The simulated results suggest that the low internal efficiency may be limited by the electron leakage current and the large nonradiative recombination we assume for the purpose of fitting the experimental output characteristics.

To further reduce the electron leakage current and improve the output characteristics, we subsequently investigate the QW number effect on the output characteristics of the UV AlGaInN LED. In this specific study, the Al composition in the AlGaN electron-block layer is 19% since our numerical analysis indicates that the best output characteristics are limited when the Al composition in the AlGaN electron-block layer is 19%. The internal loss value is set and remains unchanged at 1000 m^{-1} when varying the QW number in the range 1–11, without contemplating the increased defects by increasing the QW number during crystal growth. Figure 8 shows the *L–I* characteristic of the UV AlGaInN LED with

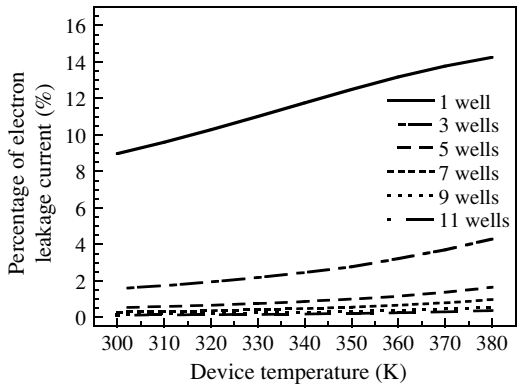

Figure 9. Percentage of electron leakage current as a function of the device temperature when the QW number is in the range 1–11.

variant QW numbers when the device temperatures are 300 K and 380 K. Figure 9 shows the percentage of electron leakage current as a function of the device temperature when the QW number is in the range of 1–11. It can be observed that the lowest output power is obtained when the QW number is 1, which is due to the large amount of electron leakage current. As the QW number increases, the output power is enhanced respectively; however, we wish to underscore that the output power at lower injection current is decreased as the QW number is more than 5, and the hole leakage is much small in the numerical analysis. Nevertheless, more QWs in the active region can undoubtedly reduce the electron leakage current and provide higher output power for higher injection current operation. Thus, numerical results suggest that the optimized QW number in the UV AlGaInN LED is in the range of 5–7.

4. Conclusion

We have fabricated a high performance 370 nm AlGaInN UV LED. The AlGaInN LED can provide an output power of 0.8 mW at 20 mA with 3.6 V operation voltage and 4 mW at 125 mA under CW operation. With the help of numerical analysis, we further investigated the effects of the Al composition in the AlGaN electron-block layer and the QW number on the 370 nm AlGaInN LED. The results obtained numerically suggest that the 370 nm AlGaInN LED can provide better output characteristics when the Al composition in the AlGaN electron-block layer is in the range 19–21% and the AlGaInN QW number is in the range 5–7. The qualitative analysis is significant for improving the output characteristics of the UV LED.

Acknowledgments

The authors would like to give their sincere appreciation to the Crosslight Incorporation for providing the advanced APSYS simulation program and professor Chia-Feng Lin of the National Chunghsing University, Taiwan, for valuable discussion. This work is supported by the National Science Council, Republic of China, under grants NSC-93-2120-M009-006 and NSC-93-2112-M-018-008, and by the Academic Excellence Program of the Ministry of Education of ROC under the contract NSC-93-2752-E009-008.

References

[1] Chitnis A *et al* 2002 *Appl. Phys. Lett.* **81** 3491
[2] Chitnis A, Zhang J-P, Adivarahan V, Shatalov M, Wu S, Pachipulusu R, Mandavilli V and Asif Khan M 2003 *Appl. Phys. Lett.* **82** 2565
[3] Han J and Nurmikko A V 2002 *IEEE J. Sel. Top. Quantum Electron.* **8** 289
[4] Pan C-C, Lee C-M, Liu J-W, Chen G-T and Chyi J-I 2004 *Appl. Phys. Lett.* **84** 5249
[5] Yasan A, McClintock R, Mayes K, Shiell D, Gautero L, Darvish S R, Kung P and Razeghi M 2003 *Appl. Phys. Lett.* **83** 4701
[6] Morita D, Sano M, Yamamoto M, Murayama T, Nagahama S and Mukai T 2002 *Japan. J. Appl. Phys.* **41** L1434
[7] Nishida T, Kobayashi N and Ban T 2003 *Appl. Phys. Lett.* **82** 1
[8] Zabelin V, Zakheim D A and Gurevich S A 2004 *IEEE J. Quantum Electron.* **40** 1675
[9] Zhang J, Yang J, Simin G, Shatalov M, Asif Khana M, Shur M S and Gaska R 2000 *Appl. Phys. Lett.* **77** 2668
[10] *APSYS User's Manual* Crosslight Inc. Software, Canada (Available online at web page http://www.crosslight.ca)
[11] Chow W-W and Koch S-W 1995 *Appl. Phys. Lett.* **66** 3004
[12] Carline R T and Allsopp D W E 1991 *Semicond. Sci. Technol.* **6** 1151
[13] Vurgaftman I and Meyer J R 2003 *J. Appl. Phys.* **94** 3675
[14] Shan W, Walukiewicz W, Haller E E, Little B D, Song J-J, McCluskey M D, Johnson N M, Feng Z-C, Schurman M and Stall R A 1998 *J. Appl. Phys.* **84** 4452
[15] Wachutka G K 1990 *IEEE Trans. Comput.-Aided Des. Integr. Circuits Syst.* **9** 1141
[16] Marshak A and Vilet K V 1978 *Solid State Electron.* **21** 417
[17] Liou L, Ebel J and Huang C 1993 *IEEE Trans. Electron Devices* **40** 35
[18] Bernardini F and Fiorentini V 2002 *Phys. Status Solidi* a **190** 65
[19] Adachi S 1987 *J. Appl. Phys.* **61** 4869
[20] Yan R-H, Corzian S W, Coldren L A and Suemune I 1990 *J. Quantum Electron.* **26** 213
[21] Piprek J, Katona T, DenBaars S P and Li S 2004 *SPIE Proc.* **5366** 127
[22] Akasaki I and Amano H 1997 *High Brightness Light Emitting Diodes* vol 48 ed G B Stringfellow and M G Craford (San Diego, CA: Academic) p 357
[23] Morkoc H, Hamdani F and Salvador A 1998 *Gallium Nitride (GaN) I* vol 50 ed J I Pankove and T D Moustakas (San Diego, CA: Academic) p 193
[24] Hansen M, Piprek J, Pattison P M, Speck J S, Nakamura S and DenBaars S P 2002 *Appl. Phys. Lett.* **81** 4275
[25] Asano T, Takeya M, Tojyo T, Mizuno T, Ikeda S, Shibuya K, Hino T, Uchida S and Ikeda M 2002 *Appl. Phys. Lett.* **80** 3497
[26] Sasanuma K and Hatakoshi G 1998 *Technical Report* LQE97-152 (Japan: IEICE)
[27] Kuo Y-K and Chang Y-A 2004 *IEEE J. Quantum Electron.* **40** 437
[28] Jeon C-W, Choi H-W, Gu E and Dawson M D 2004 *IEEE Photon. Technol. Lett.* **16** 2421
[29] Morita D, Sano M, Yamamoto M, Nonaka M, Yasutomo K, Akaishi K, Nakahama S and Mukai T 2003 *Phys. Status Solidi* a **200** 114
[30] Adivarahan V, Chitinis A, Zhang J-P, Shatalov M, Yang J-W, Simin G and Asif Khan M 2001 *Appl. Phys. Lett.* **79** 4240
[31] Kim K-H, Fan Z-Y, Khizar M, Nakarmi M L, Lin J-Y and Jiang H-X 2004 *Appl. Phys. Lett.* **85** 4777